Dynamic Study of Single-Chain Adsorption and Desorption

Niklas Källrot* and Per Linse

Physical Chemistry 1, Center for Chemistry and Engineering, Lund University, P.O. Box 124, S-221 00 Lund, Sweden

Received January 30, 2007; Revised Manuscript Received April 17, 2007

ABSTRACT: The dynamics of adsorption and desorption of uncharged homopolymers have been investigated using a coarse-grained model comprised of a bead−spring chain and a planar surface. Brownian dynamics simulation has been used to examine the adsorption process for polymers released near the surface and with bulk properties as well as Monte Carlo simulations to explore equilibrium adsorption structures of the polymer. Systems with varying polymer contour length, polymer stiffness, and polymer−surface interaction potential have been considered. Investigations have been made on polymer extensions perpendicular and parallel to the surface and also characterized the adsorbed state in terms of loops, tails, and trains. After a diffusion of the polymer to the vicinity of the surface, three succeeding phases were identified: distortion, attachment, and relaxation phase. In the distortion phase, the polymer starts to experience the potential of the surface and becomes elongated perpendicular to the surface. In the attachment phase, the polymer makes direct contact with the surface and becomes contracted perpendicular to the surface and starts to spread on the surface. Finally, in the extended relaxation phase, the polymer continues to spread on the surface.

1. Introduction

Polymers in solution placed in contact with a surface may adsorb to the surface if there is an attractive polymer−surface interaction exceeding the entropy loss associated with the adsorption.[1] Such an adsorption process may be governed by properties of the surface, the polymer, or the solvent as well as the fine interplay among these. Adsorption of polymers onto solid interfaces is fundamental in a wide range of applications and has therefore received substantial interest for a long time. Controlling polymer adsorption onto solid surfaces is a key issue in many technical areas such as the paper industry, pharmaceutical applications, and in paint formulations.[2]

Polymer adsorption has been studied extensively using different experimental techniques, and there is a vast amount of material available on structures of adsorbed polymers, such as surface coverage and layer thickness.[3] In many cases, the kinetics is slow, and it is questionable whether a full equilibrium is established, even after very long times. Moreover, it is not always clear what influence the initial stages of an adsorption process may have on the final structures of an adsorbed layer.

The transition of a polymer from bulk solution to being fully adsorbed can be regarded as a stepwise process involving several stages comprising different time scales. Initially, a polymer must diffuse to the vicinity of the surface, possibly through a stagnant layer. When the polymer is in close enough proximity to the surface, the attraction between the polymer segments nearest the surface will pull these segments toward the surface, leading to an adsorption kinetics faster than bulk diffusion. When the polymer as a whole has been transported to the surface by the attraction, the polymer will collapse onto the surface and start to spread on it, establishing a quasi-two-dimensional-like structure if the polymer−surface attraction is strong.[4] The reorganization on the surface is very slow and is in many systems believed to be kinetically trapped.

Various theoretical approaches such as mean-field theories and simulation methods have been employed to describe and model polymer adsorption employing coarse-grained models. A simple but important kinetic model of polymer adsorption and desorption has been proposed,[5] and dynamic mean-field theory has been used to examine adsorption of polymers from solution.[6] Simulation methods have been employed to investigate static properties of single polymers adsorbed onto solid surfaces,[7−15] and in other investigations dynamic aspects were also included.[16−28] Some of the dynamical investigations involved adsorption of a single polymer[17,24,26] and of polymers from solution from nonequilibrium states.[16] However, most of the investigations deal with the dynamics of equilibrium systems,[18−23,25,27,28] and an important issue in many of these papers is the examination of the detachment dynamics inspired by the work in ref 5. A few related theoretical and simulation studies have dealt with the adsorption of polyelectrolytes onto planar surfaces.[30−32] The coarse-graining involved either a lattice (mostly a cubic)[7,9,11,14,15,17−21,25,26,28] or a chain of segments, freely jointed[12,13,31] or connected with harmonic,[8,32] finite extensible,[22−24] or LJ-type[10] bonds. The Monte Carlo simulation techniques were used in most of these studies; in some of the dynamics investigation also nonlocal trial moves were employed which, however, made the dynamical results less rigorous.[16,21,25,28] In other studies, molecular dynamics or Brownian dynamics techniques were used.[8,10,24]

It is plausible that a better knowledge of the initial behavior of the adsorption process may contribute to better understanding of adsorbed (equilibrium) structures at longer times. From a biological standpoint there is also interest in adsorption dynamics, since adsorption often induces conformational changes in biopolymers.[29]

In this study, a coarse-grained bead−spring model is employed to study the dynamics of single polymer chains adsorbing onto and desorbing from a planar surface using Brownian dynamic simulations. A number of different systems have been examined, including different chain length, chain stiffness, and chain−surface interaction potential. Equilibrium structures of these systems have also been examined using Monte Carlo simulation techniques. In comparison with previous studies on single-polymer adsorption, where the dynamics were investi-

* Corresponding author. E-mail: Niklas.Kallrot@fkem1.lu.se.

10.1021/ma0702602 CCC: $37.00
Published on Web 06/05/2007

gated with the polymer already in contact with the surface,[17,24,26] the polymers were released close to the surface, and significant conformational changes appeared before physical contact emerged. Moreover, the dynamics of the contraction perpendicular to the surface and the subsequent spreading on the surface were examined, and the kinetics of the loop, tail, and train formation were analyzed. Finally, single-polymer adsorption as studied in this work may apply to adsorption from very dilute polymer solutions but is more directly comparable with techniques developed for single molecular resolution.[33]

2. Model

A simple coarse-grained model is used to investigate the dynamics of single polymers adsorbing onto and desorbing from a smooth and planar surface. The polymer is represented by a chain of N spherical beads connected via harmonic potentials. The stiffness of the chain is regulated through harmonic angular potentials. The polymer is confined in a cubic box with edge length L. Periodic boundaries are applied in the x and y directions, and the planar surface is located at $z = 0$. The boundary condition at $z = L$ is irrelevant because only polymers close to the surface at $z = 0$ are examined.

The total potential energy U of the system can be expressed as a sum of four different terms: nonbonded bead−bead potential energy U_{nonbond}, bonded potential energy U_{bond}, angular potential energy U_{angle}, and a bead−surface potential energy U_{surf}, according to

$$U = U_{\text{nonbond}} + U_{\text{bond}} + U_{\text{angle}} + U_{\text{surf}} \tag{1}$$

The nonbonded bead−bead potential energy is assumed to be pairwise additive according to

$$U_{\text{nonbond}} = \sum_{i<j}^{N} u(r_{ij}) \tag{2}$$

where the truncated and shifted repulsive Lennard-Jones (LJ) potential energy

$$u(r_{ij}) = \begin{Bmatrix} 4\epsilon\left[-\left(\frac{\sigma}{r_{ij}}\right)^6 + \left(\frac{\sigma}{r_{ij}}\right)^{12} + \frac{1}{4}\right], & r_{ij} \le 2^{1/6}\sigma \\ 0, & r_{ij} > 2^{1/6}\sigma \end{Bmatrix} \tag{3}$$

is used for the interaction between beads i and j, with r_{ij} being the distance between the two beads, $\sigma = 3.405$ Å the diameter of the bead, and $\epsilon = 0.9961$ kJ/mol the interaction strength. In the presence of all interactions, the root-mean-square (rms) bead−bead separation of bonded beads becomes $\langle R_{\text{bb}}^2\rangle^{1/2} \approx 5.6$ Å.

The bond and angular potential energies are given by

$$U_{\text{bond}} = \frac{1}{2}k_{\text{bond}}\sum_{i=1}^{N-1}(r_i - r_{\text{eq}})^2 \tag{4}$$

$$U_{\text{angle}} = \frac{1}{2}k_{\text{angle}}\sum_{i=2}^{N-1}(\theta_i - \theta_{\text{eq}})^2 \tag{5}$$

where $k_{\text{bond}} = 2.4088$ kJ/mol is the bond force constant and k_{angle} the angular force constant that determines the stiffness of the chain. Moreover, $r_{\text{eq}} = 5.0$ Å represents the equilibrium bond length and $\theta_{\text{eq}} = 180°$ the equilibrium bond angle.

The polymer−surface interaction is taken as a sum of bead−surface interactions according to

$$U_{\text{surf}} = \sum_{i=1}^{N} u_{\text{surf}}(z_i) \tag{6}$$

where an attractive 3−9 LJ potential

$$u_{\text{surf}}(z_i) = \frac{2\pi}{3}\rho_s\sigma_s^3\epsilon_s\left[-\left(\frac{\sigma_s}{z_i}\right)^3 + \frac{2}{15}\left(\frac{\sigma_s}{z_i}\right)^9\right] \tag{7}$$

is used for the interaction between bead i and the surface in the adsorption simulations and a shifted and truncated repulsive 3−9 LJ potential[27]

$$u_{\text{surf}}(z_i) = \begin{Bmatrix} \frac{2\pi}{3}\rho_s\sigma_s^3\epsilon_s\left[-\left(\frac{\sigma_s}{z_i}\right)^3 + \frac{2}{15}\left(\frac{\sigma_s}{z_i}\right)^9 + \left(\frac{\sqrt{10}}{3}\right)\right], & z_i \le \left(\frac{2}{5}\right)^{1/6}\sigma_s \\ 0, & z_i > \left(\frac{2}{5}\right)^{1/6}\sigma_s \end{Bmatrix} \tag{8}$$

for the desorption studies. In eqs 7 and 8, ρ_s is the density of the (hypothetical) particles forming the surface, σ_s the mean diameter of beads and surface particles, ϵ_s a potential energy parameter describing the bead−surface interaction, and z_i the z-coordinate of bead i. For simplicity, $\sigma_s = 3.5$ Å and $\rho_s\sigma_s^3 = 1$ were chosen. With the attractive 3−9 LJ potential, the potential minimum appears at $z_{\text{min}} = (2/5)^{1/6}\sigma_s \approx 3.0$ Å and amounts to $u_{\text{surf}}(z_{\text{min}}) = -[2\pi(10)^{1/2}/9]\rho_s\sigma_s^3\epsilon_s \approx -2.2\epsilon_s$. In addition to the LJ potential, a weak external potential linear in z [$U_{\text{ext}}(z) = Az$, $A = 0.08$ kJ/(mol Å)] was included to promote the motion of the polymer toward the surface. The magnitude of the external force $F_{\text{ext}} = -A$ should be compared with the most negative value of the bead−surface force appearing at $z = \sigma_s$, $F_{\text{surf}}(z = \sigma_s) = -(6\pi/5)\rho_s\sigma_s^2\epsilon_s \approx -2.7$ kJ/(mol Å).

One system consisting of a polymer with $N = 40$ beads, angular force constant $k_{\text{angle}} = 0$, and the bead−surface potential energy parameter $\epsilon_s = 2.5$ kJ/mol will be used as the reference system throughout this work. In addition, polymers with (i) chain lengths $N = 80$, 160, 320, and 640 beads, (ii) angular bond constants $k_{\text{angle}} = 1.2$ and 10 J/(mol deg^2), and (iii) bead−surface interaction parameter $\epsilon_s = 6.0$ kJ/mol are considered. The variation of k_{angle} leads to polymers with different flexibility. The intrinsic flexibility was characterized by calculating the persistence length based on the local folding l_p of a single polymer without surface according to $l_p = \langle R_{\text{bb}}^2\rangle^{1/2}/(1 + \langle\cos\theta\rangle)$.[34,35] The persistence length for the polymers with the different angular force constants became $l_p \approx 7$, 13, and 77 Å, respectively. Data describing the model systems are collected in Table 1.

3. Method

Two different simulation techniques have been used. Brownian dynamics (BD) simulation was employed to examine the adsorption and desorption dynamics, whereas Monte Carlo (MC) simulations were used to generate equilibrated polymer configurations and to determine equilibrium properties of adsorbed and desorbed polymers. All simulations were carried out using the canonical (NVT) ensemble, characterized by a constant number of particles, volume, and temperature.

The adsorption simulation studies involved three steps: (i) First, an equilibrated polymer conformation without influence of any surface was generated by MC simulation. (ii) Thereafter, the polymer was placed near the adsorbing surface located at $z = 0$ (cf. eqs 6−8), such that the distance between the bead closest to the surface and the surface was 12 Å. A larger separation would increase the time for the polymer to diffuse

Table 1. Model Parameters[a]

cubic box length	$L = 1000$ Å
temperature	$T = 298$ K
no. of beads in a chain	$N = 40$, 80, 160, 320, and 640
bead−bead LJ parameter	$\sigma = 3.405$ Å
bead−bead LJ parameter	$\epsilon = 0.9961$ kJ/mol
force constant of bond potential	$k_{bond} = 2.4088$ kJ/mol
force constant of angle potential	$k_{angle} = 0$, 1.2, and 10 J/(mol deg^2)
equilibrium separation of bond potential	$r_{eq} = 5.0$ Å
equilibrium angle of angle potential	$\theta_{eq} = 180°$
bead−surface LJ parameter	$\sigma_s = 3.5$ Å
bead−surface LJ parameter	$\epsilon_s = 2.5$ and 6.0 kJ/mol

[a] Despite the use of a generic model, the use of real units is retained. This will be advantageous in future studies.

to the surface, and a smaller distance would lead to an initial polymer configuration not in conformational equilibrium with the surface potential. It should be noted that in this work the polymers have been placed such that they have the same closest distance to the surface. Obviously, another approach would have been to have the same distance between the center of mass and the surface. These two approaches are not equivalent when comparing the adsorption of polymers of different size (varying N) or shapes (varying k_{angle}). (iii) Finally, the BD simulation was performed. For each system, averages over ≈1000 such adsorption simulations were made, using uniquely equilibrated polymer configurations. Simulations, in which the polymer did not adsorb after ≈2.4 ps (ca. 15% of the cases), were not included in the subsequent analysis in order to reduce the spread in the surface arrival time of the polymers.

The desorption studies involved two steps and were performed in a similar manner: (i) An equilibrated configuration of an adsorbed polymer was generated by MC simulation using the attractive bead−surface potential (eq 7). (ii) Thereafter, the BD simulation was performed using the shifted and truncated repulsive 3−9 LJ potential (eq 8). Also here, an averaging over ≈1000 individual simulations with different equilibrated polymer conformations was made. Different bead−surface potentials are used for the adsorption and desorption processes, so these processes are not the reverse of each other.

In the BD simulations, the motion of the polymer beads was described by[36]

$$\mathbf{r}_i(t+\Delta t) = \mathbf{r}_i(t) + \frac{D_0 \Delta t}{kT}\mathbf{F}_i(t) + \mathbf{R}_i(t;\Delta t) \qquad (9)$$

where $\mathbf{r}_i(t+\Delta t)$ is the location of bead i at the time $t + \Delta t$, $\mathbf{r}_i(t)$ the location of bead i at the time t, D_0 the bead self-diffusion coefficient in the absence of systematic forces, k Boltzmann's constant, T the temperature, and $\mathbf{F}_i(t)$ the systematic force on bead i at time t arising from the potential energy U given by eq 1. Furthermore, $\mathbf{R}_i(t;\Delta t)$ is a random displacement of bead i representing the effect of collisions with solvent molecules at time t and sampled from a Gaussian distribution with the mean $\langle \mathbf{R}_i(t;\Delta t)\rangle = 0$ and the variance $\langle \mathbf{R}_i(t;\Delta t)\cdot\mathbf{R}_j(t';\Delta t)\rangle = 6D_0\Delta t\delta_{ij}\delta(t - t')$ as obtained from the fluctuation−dissipation theorem. In this work, hydrodynamic interactions are neglected.

A bead self-diffusion coefficient $D_0 = 0.1$ Å^2/ps was used, and an integration time step $\Delta t = 0.05$ ps was employed. The BD simulations involved 5×10^6 time steps, providing a nominal simulation time of 250 ns. Using $\tau_{BD} = \sigma^2/D_0 = 116$ ps as the conventional unit of time, the integration time step becomes $\Delta t = 0.004\tau_{BD}$ and the total simulation time $21000\tau_{BD}$.

The MC simulations were performed according to the Metropolis algorithm,[37] using two different types of trial moves: (i) translation of individual beads and (ii) pivot rotation of a subchain of the polymer. The translational displacement parameter was 3 Å, and the probability of a pivot rotation was $1/N$ of that of a single-bead trial move. The MC simulations comprised 2×10^7 trial moves per bead after equilibration. All simulations presented in this work were performed using the integrated Monte Carlo/molecular dynamics/Browninan dynamics simulation package MOLSIM.[38]

4. Structural and Dynamical Analysis

The dynamics of the adsorption and desorption processes were examined by several time-dependent quantities. The location of the polymer at time t was described using the center of mass $\mathbf{r}_{com}(t)$ defined according to

$$\langle \mathbf{r}_{com}(t)\rangle = \left\langle \frac{1}{N}\sum_{i=1}^{N} \mathbf{r}_i(t) \right\rangle \qquad (10)$$

where $\mathbf{r}_i(t) = [x_i(t), y_i(t), z_i(t)]$ is the coordinate of bead i at time t. Here and in the following, $\langle ... \rangle$ denotes the average over the ≈1000 independent simulations. In particular, the location of the center of mass along the z-axis, $\langle z_{com}(t)\rangle$, obtained by replacing $\mathbf{r}_i(t)$ by $z_i(t)$ in eq 10 will be important.

The three-dimensional extension of the polymer at time t is described by its rms radius of gyration $\langle R_g^2(t)\rangle^{1/2}$ defined according to

$$\langle R_g^{\,2}(t)\rangle = \left\langle \frac{1}{N}\sum_{i=1}^{N} [\mathbf{r}_i(t) - \mathbf{r}_{com}(t)]^2 \right\rangle \qquad (11)$$

The transition from bulk to an adsorbed state involves structural rearrangements of the polymer, essentially from a 3- to 2-dimensional object. The perpendicular ($\perp$) and parallel ($||$) projection to the surface of $\langle R_g^2(t)\rangle$ is considered according to

$$\langle R_g^{\,2}(t)\rangle_\perp = \left\langle \frac{1}{N}\sum_{i=1}^{N} [z_i(t) - z_{com}(t)]^2 \right\rangle \qquad (12)$$

$$\langle R_g^{\,2}(t)\rangle_{||} = \left\langle \frac{1}{N}\sum_{i=1}^{N} \{[x_i(t) - x_{com}(t)]^2 + [y_i(t) - y_{com}(t)]^2\} \right\rangle \qquad (13)$$

satisfying $\langle R_g^2(t)\rangle = \langle R_g^2(t)\rangle_\perp + \langle R_g^2(t)\rangle_{||}$.

A polymer was considered as being adsorbed if at least one bead was in contact with the surface, here defined by $z_i < 6$ Å. Remember that the minimum of the bead−surface potential is located at $z_{min} \approx 3$ Å. The structure of adsorbed polymers was described by using loop, tail, and train subchains.[3] A subchain of adsorbed beads is referred to as a train, a nonadsorbed subchain with both ends bonded to trains as a loop, and a nonadsorbed subchain with one end bonded to a train as a tail. The average total number of beads in subchains of type α at time t will be denoted by $\langle N_\alpha(t)\rangle$, the average number of subchains of type α at time t by $\langle n_\alpha(t)\rangle$, and the average number of beads in a subchain of type α at time t by $\langle L_\alpha(t)\rangle$ with α = {loop, tail, train}. By conservation: (i) $\sum_\alpha \langle N_\alpha(t)\rangle = N$, (ii) $\langle n_{train}(t)\rangle = \langle n_{loop}(t)\rangle + 1$, and (iii) $\langle N_\alpha(t)\rangle = \langle n_\alpha(t)L_\alpha(t)\rangle \approx \langle n_\alpha(t)\rangle\langle L_\alpha(t)\rangle$.

The time dependence of the local folding of chains is also examined. This will be characterized by the average angle between three consecutive beads at time t, denoted by $\langle\theta(t)\rangle$.

Finally, the relaxation of some of these properties from their initial values to their equilibrium values was examined. That was performed by monitoring

$$q(t) = \frac{\langle X(t)\rangle - X_{eq}}{\langle X(0)\rangle - X_{eq}} \tag{14}$$

where $X(t)$ denotes the value of property X at time t, $X(0)$ its value at time $t = 0$, and X_{eq} its equilibrium value. From the slope of ln $q(t)$ vs t, the relaxation time of the corresponding process was extracted.

5. Bulk Solution

In addition to the adsorption and desorption simulations, complementary simulations of a single and flexible polymer in an infinitely dilute solution have been performed at various chain lengths to characterize our polymer model. From such MC simulations with $N = 40$, 80, 160, 320, and 640, it was found that $\langle R_g^2\rangle^{1/2} \sim N^{\nu}$ with $\nu \approx 0.59 \pm 0.01$, in agreement with the theoretical prediction $\nu = 0.588$ for chains in a good solvent.[39] Dynamic analyses of corresponding BD dynamic simulations involving 1×10^8 time steps with $N = 10$, 20, 40, 80, and 160 gave a chain self-diffusion coefficient D consistent with $D = D_0N^{-1}$, as predicted for Rouse dynamics.[17] The internal relaxation of the chain was examined in terms of the end-to-end vector time correlation function (the first Legendre polynomial). The time correlation function was fitted to an exponential decaying function with the relaxation time τ_R. The relation $\tau_R \sim N^{\alpha}$ was obtained with the relaxation time $\tau_R = 1.0$ ns for $N = 10$ and $\alpha = 2.5 \pm 0.2$, the latter being slightly larger than the exponent given by Shaffer,[17] $\alpha = 1 + 2\nu$ with $\nu = 0.588$ for Rouse dynamics in a good solvent.

6. Adsorption

The adsorption processes of the reference system will first be examined. Thereafter, the influence of the chain length, chain stiffness, and bead−surface interaction will be considered.

6.1. Reference System. As previously mentioned, a single polymer equilibrated in the absence of the surface was brought near the surcface with the smallest bead−surface separation equal to 12 Å. The initial rms radius of gyration was $\langle R_g^2\rangle^{1/2} \approx 19$ Å, and the initial location of the center of mass of the polymer became $\langle z_{com}\rangle \approx 27$ Å.

First, the time required for the chain to diffuse to the surface and make the first bead−surface contact under the influence of the bead−surface attraction and the external potential was established. Figure 1 shows the normalized probability $P(t_A)$ of the time t_A required for this process. The distribution peaks at 0.5 ns. About 45% of the polymers are adsorbed after 1 ns and 85% after 2.4 ns, the later time being the upper limit for including the simulation in the averaging. The dispersion in the arrival time is small as compared to subsequent and slower processes, making the averaging of these processes only marginally affected by this dispersion.

Figure 2 displays the center of mass in the z-direction, the rms radius of gyration, and its two projections for the polymer as functions of simulation time. The initial part is given on a linear time scale (Figure 2a), whereas the full adsorption process is given on a logarithmic time scale (Figure 2b).

Starting with the translational motion of the center of mass, the displacement during the initial ≈3 ns is linear in time and amounts to ≈10 Å. For the majority of the beads, the external force dominates over the surface 3−9 LJ force, and the drift velocity is in agreement with $v_{ext} = D_0F_{ext}/kT \approx 3.4$ Å/ns. At longer times, the drift velocity decreases and $\langle z_{com}(t)\rangle$ approaches 1.9 Å at $t \approx 15$ ns. Initially, $\langle R_g^2(t)\rangle_{\perp}^{1/2}$ increases weakly but then displays a maximum at $t \approx 2$ ns and approaches ≈2 Å also at $t \approx 15$ ns. Finally, $\langle R_g^2(t)\rangle_{\parallel}^{1/2}$ is initially constant but starts to increase steadily after ≈4 ns. Noticeably, its increase continues after $t \approx 15$ ns, the time at which the diffusion in the z-direction and the change in the perpendicular extension has stopped. After the initial increase, $\langle R_g^2(t)\rangle_{\perp}^{1/2}$ relaxes exponentially toward its equilibrium value with a relaxation time $\tau_{\perp} = 2.9$ ns. The relaxation of $\langle R_g^2(t)\rangle_{\parallel}^{1/2}$ involves two separate modes with the relaxation times $\tau_{\parallel} = 14$ and 52 ns, respectively; the first modes comprises 90% of the relaxation. Because of the

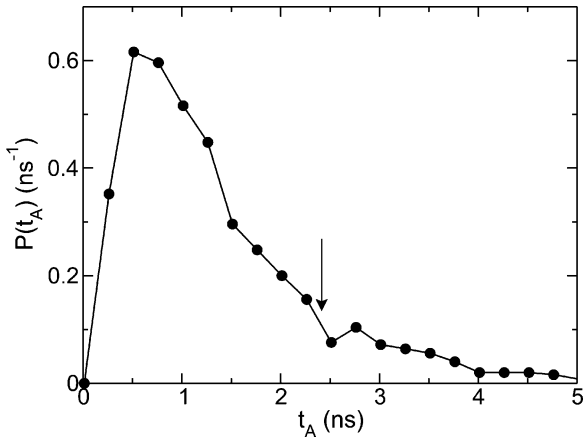

Figure 1. Normalized probability distribution $P(t_A)$ of arrival time t_A for a polymer released with a smallest bead−surface separation equal to 12 Å for the reference system. The arrow indicates the upper time limit at which polymers are included in the analyses.

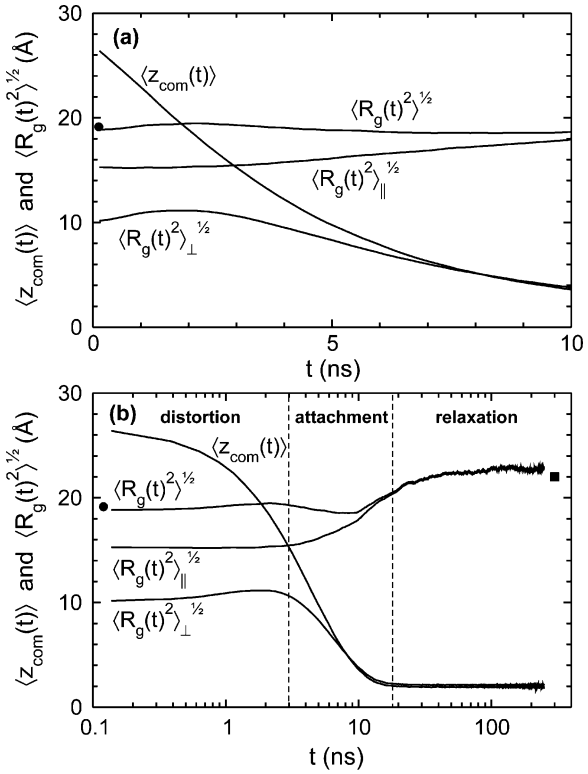

Figure 2. Center of mass $\langle z_{com}(t)\rangle$, rms radius of gyration $\langle R_g^2(t)\rangle^{1/2}$, and its two projections $\langle R_g^2(t)\rangle_{\perp}^{1/2}$ and $\langle R_g^2(t)\rangle_{\parallel}^{1/2}$ as a function of time t for the reference system during adsorption with (a) linear and (b) logarithmic time scale. Rms radius of gyration for free polymer (circles) and adsorbed polymer (square) obtained from MC simulations are also shown. In (b), the three characteristic phases of the adsorption process are also given.

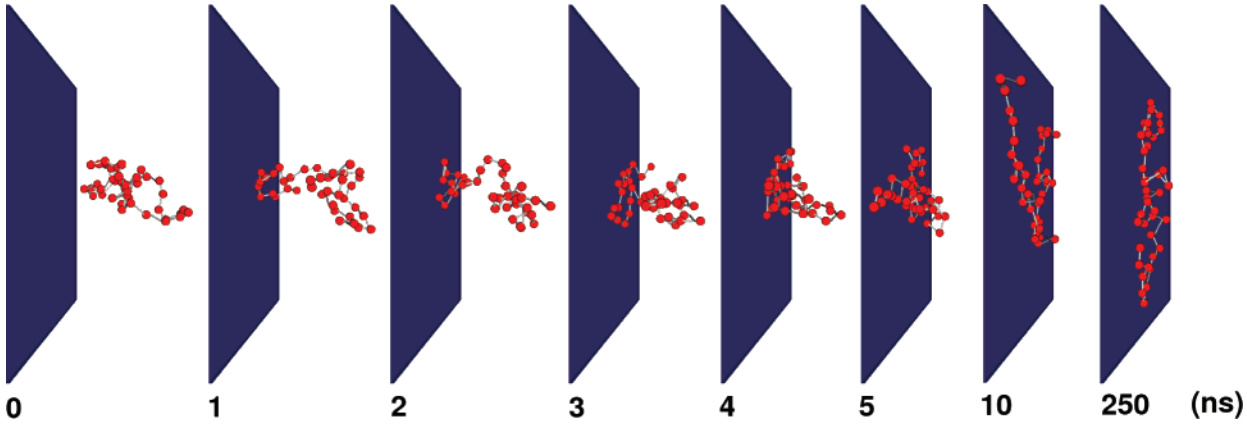

Figure 3. Snapshots from a BD simulation illustrating the adsorption process for the reference system. Note, the largest structural rearrangements are established within the first 10 ns of the 250 ns long simulation.

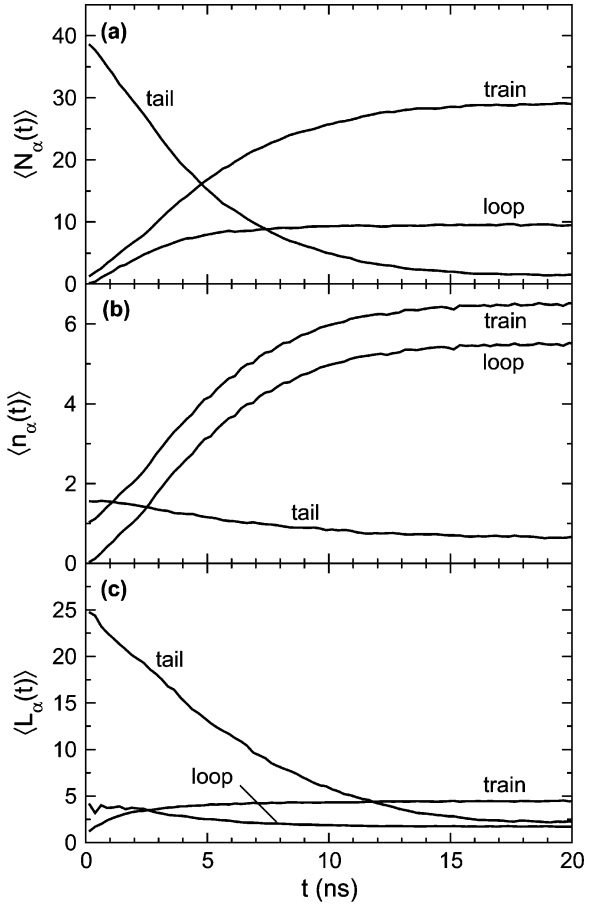

Figure 4. (a) Average total number of beads being in loops, tails, and trains $\langle N_\alpha(t)\rangle$, (b) average number of loops, tails, and trains $\langle n_\alpha(t)\rangle$, and (c) average number of beads in a loop, tail, and train $\langle L_\alpha(t)\rangle$, $\alpha = \{\text{loop, tail, train}\}$ as a function of time t for the reference system during adsorption.

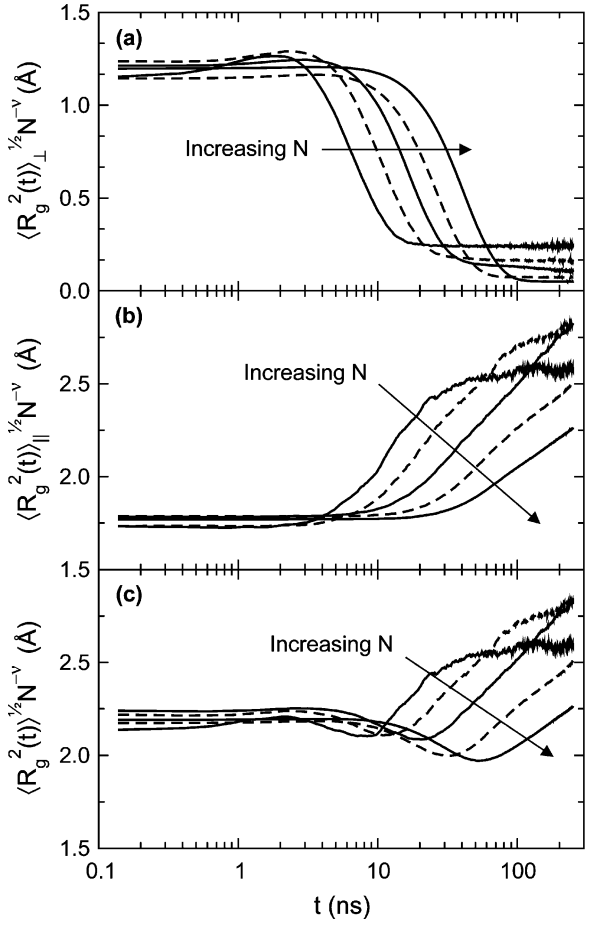

Figure 5. (a) Normalized rms radius of gyration perpendicular to the adsorbing surface $\langle R_g^2(t)\rangle_\perp^{1/2}N^{-\nu}$, (b) normalized rms radius of gyration parallel to the adsorbing surface $\langle R_g^2(t)\rangle_\parallel^{1/2}N^{-\nu}$, and (c) normalized rms radius of gyration $\langle R_g^2(t)\rangle^{1/2}N^{-\nu}$ as a function of time t during adsorption for polymers with $N = 40$, 80, 160, 320, and 640 beads and $\nu = 0.59$.

nonmonotonic behavior of $\langle R_g^2(t)\rangle_\perp^{1/2}$ and the increase of $\langle R_g^2(t)\rangle_\parallel^{1/2}$ after $\langle R_g^2(t)\rangle_\perp^{1/2}$ has started to decrease, $\langle R_g^2(t)\rangle^{1/2}$ displays first a local maximum and then a minimum before it reaches its final value. The rms radius of gyration at $t = 250$ ns agrees with that obtained from the independent MC simulation (square in Figure 2b). In Figure 3 snapshots from one single BD simulation have been extracted, displaying the adsorption process at different times.

On the basis of these results the observed adsorption process is divided into three phases, viz. (i) a distortion phase, (ii) an attachment phase, and (iii) a relaxation phase (see Figure 2b). (i) The distortion phase comprises the first ≈3 ns, during which the chain is diffusing to the surface under the influence of the bead−surface and external forces. The polymer is not yet, or only slightly, in physical contact with the surface. Nevertheless, the chain is extended perpendicular toward the surface due to the influence of the attraction between the beads being closest to the surface and the surface. This effect would probably be more accentuated without the external force. (ii) The attachment phase extends to $t \approx 15$ ns and involves a chain contraction perpendicular to the surface, ending up in a conformation where the chain is essentially 2-dimensional, i.e., $\langle R_g^2\rangle_\perp^{1/2} < \langle R_{bb}^2\rangle^{1/2}$. During this phase, the chain also starts to expand parallel to

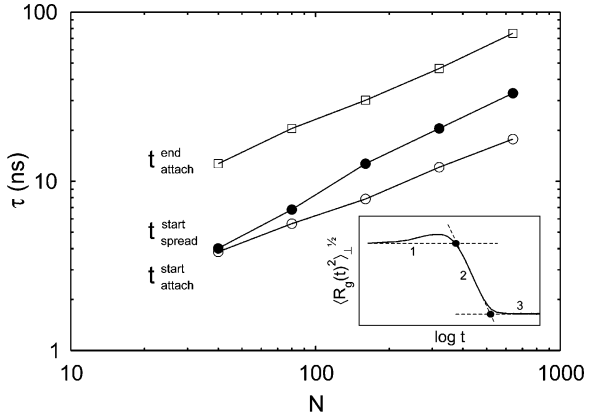

Figure 6. Start of the attachment phase $t_{\text{attach}}^{\text{start}}$, end of the attachment phase $t_{\text{attach}}^{\text{end}}$, and the start of the spreading of the polymer on the surface as a function of the chain length N during adsorption. The inset shows schematically the evaluation of $t_{\text{attach}}^{\text{start}}$ as the intersect between lines 1 and 2 and $t_{\text{attach}}^{\text{end}}$ as the intersect between lines 2 and 3.

Table 2. Equilibrium Values of $\langle R_g^2 \rangle_\perp^{1/2}$ and $\langle R_g^2 \rangle_\parallel^{1/2}$ for Adsorbed Polymers from the MC Simulations[a]

label	N	k_{angle} (J/(mol deg^2))	ϵ_s (kJ/mol)	$\langle R_g^2 \rangle_\perp^{1/2}$ (Å)	$\langle R_g^2 \rangle_\parallel^{1/2}$ (Å)
Ref	40	0	2.5	2.64	21.4
	80	0	2.5	2.65	34.8
	160	0	2.5	2.67	62.1
	320	0	2.5	2.66	99.8
	640	0	2.5	2.64	184.3
A1	40	1.2	2.5	2.17	32.5
A2	40	10	2.5	0.73	52.5
E1	40	0	6.0	0.79	25.5

[a] Largest estimated uncertainties for the rms radius of gyration are 4%.

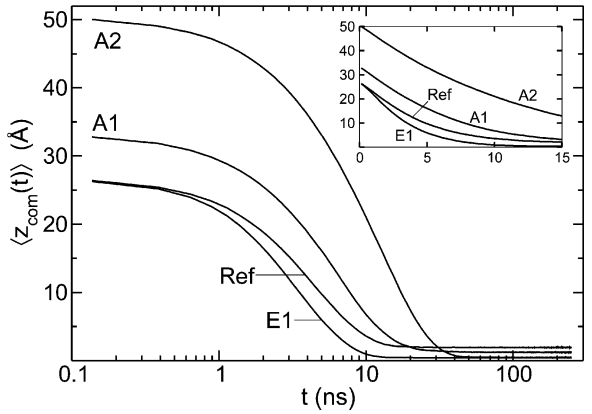

Figure 7. Center of mass $\langle z_{\text{com}}(t) \rangle$ for the reference system (Ref), the semiflexible polymer (A1), the stiff polymer (A2), and the polymer with the stronger bead−surface attraction (E1) during adsorption. The inset displays the linear behavior mainly in the distortion and the attachment phase.

the surface. (iii) During the relaxation phase, the polymer continues to spread over the surface but at constant perpendicular extension. The relaxation phase extends to $t \approx 100$ ns and is thus 1 order of magnitude longer than the attachment phase.

Below, the time evolution of the formation of loops, tails, and trains for adsorbed chains is considered. Figure 4 displays the average number of beads in the three types of subchains $\langle N_\alpha(t) \rangle$, the average number of the different types of subchains $\langle n_\alpha(t) \rangle$, and the average number of beads in a subchain of the different types $\langle L_\alpha(t) \rangle$. It should be stressed the data given comprise adsorbed chains only.

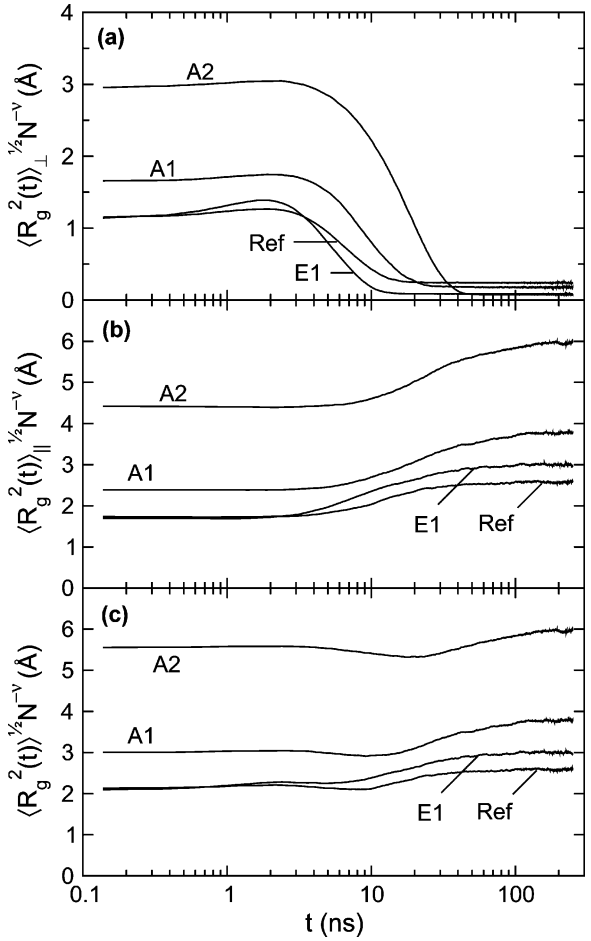

Figure 8. (a) Normalized radius of gyration perpendicular to the adsorbing surface $\langle R_g^2(t) \rangle_\perp^{1/2} N^{-\nu}$, (b) normalized radius of gyration parallel to the adsorbing surface $\langle R_g^2(t) \rangle_\parallel^{1/2} N^{-\nu}$, and (c) normalized radius of gyration $\langle R_g^2(t) \rangle^{1/2} N^{-\nu}$ as a function of time t for the reference system (Ref), the semiflexible polymer (A1), the stiff polymer (A2), and the polymer with the stronger bead−surface attraction (E1) during adsorption.

At the initial stage of the adsorption process, nearly all beads in the adsorbed polymer reside in tails (Figure 4a); 1.6 tails and 1 train are present (Figure 4b), and an average tail involves 24 beads (Figure 4c). These data imply that the polymer displays essentially only one single contact with the surface. Furthermore, the probability for either of the two end beads to be adsorbed is enhanced, since equal probability for $N = 40$ beads implies $\langle n_{\text{tail}} \rangle = 2(1 - 1/N) = 1.95$ and $\langle L_{\text{tail}} \rangle = (N - 1)(1/2 + 1/N) \approx 20.5$.

In the attachment phase, the characteristics of the loops, tails, and trains change drastically. The number of beads residing in tails drops to about one, whereas the number of beads in loops and trains becomes 10 and 29, respectively (Figure 4a). The transition of beads from tails to loops and to trains is linear in time up to $t \approx 5$ ns. The number of beads in loops levels off at $t = 10$ ns, whereas the conversion of beads residing in tails to trains continues to $t \approx 20$ ns. The relaxation of $\langle N_{\text{tail}} \rangle$ toward its equilibrium value is in the attachment phase nearly exponential with a relaxation time $\tau_{N_{\text{tail}}} = 4$ ns. Moreover, the average number of tails decreases from 1.6 to 0.7 and the number of loops and trains increase to 5.5 and 6.5, respectively (Figure 4b). Finally, the average length of a tail decreases from 24 to 2 beads and the length of a loop becomes 2 beads, whereas the length of a train increases to 5 beads (Figure 4c).

All the changes of the subchain characteristics are completed after $t \approx 20$ ns. Hence, these characteristics remain essentially

constant in the relaxation phase that follows the attachment phase. Hasegawa and Doi[6] have presented a related analysis of polymer adsorption from solution using a dynamic mean-field theory. They obtained a similar qualitative time dependence of the loop, tail, and train characteristics. The main difference was that they observed what they refer to as a second stage of the adsorption process, during which, e.g., the length of the tails and loops increased and the length of the trains decreased. This behavior was rationalized by the crowding effect appearing at the surface during the later stage of the adsorption process. The effect was more pronounced in a poor solution where the adsorbed equilibrium amount is larger.

In summary, the adsorption process has been split into three phases according to the dominating structural changes. In the distortion phase, the polymer approaches the surface and becomes slightly extended perpendicular to the surface due to the fact that the surface attracts nearby beads stronger than more distant beads. The magnitude of this effect depends on the balance between the force gradient near the surface and the internal coil relaxation rate. In the attachment phase, the polymer undergoes drastic conformational changes. It becomes quasi-two-dimensional and establishes roughly 6 anchoring subchains consisting of ≈5 beads, separated by loops of ≈2 beads each. The length of the tails is negligible. In the final relaxation phase, the chain continues to expand slowly over the surface driven by bead−bead excluded volume interactions, but its perpendicular extension, as well as its loop, tail, and train characteristics, remains unaltered.

6.2. Variation of Chain Length. In the following section the adsorption process is investigated with respect to the polymer length. This is done by considering polymers with $N = 40$, 80, 160, 320, and 640 beads.

Figure 5 displays the normalized rms radius of gyration and its two projections. Here, these functions have been normalized with N^{ν} with $\nu = 0.59$, obtained from the bulk simulations, making their initial values essentially N independent. This shows that qualitative time dependencies of $\langle R_g^2(t)\rangle^{1/2}$, $\langle R_g^2(t)\rangle_{\perp}^{1/2}$, and $\langle R_g^2(t)\rangle_{\parallel}^{1/2}$ are independent of N. The main difference is that the increase in polymer size leads to slower dynamics. Unfortunately, for $N \geq 40$ the full relaxation phase could not be simulated.

More specifically, Figure 5a shows that the initial increase of $\langle R_g^2(t)\rangle_{\perp}^{1/2}$ occurs also for longer chains. However, the effect becomes smaller at increasing N, which shows that as the number of beads initially extended toward the surface is basically independent of N, the remaining part of the chain increases with N. Despite the slower dynamics, even for the longest chain, $\langle R_g^2(t)\rangle_{\perp}^{1/2}$ is able to reach its asymptotic value before the end of the simulation. Thus, the complete attachment phase could still be covered. The relaxation of $\langle R_g^2(t)\rangle_{\perp}^{1/2}$ toward its equilibrium value is exponential for $N = 40$, 80, and 160 down to a relative amplitude of 0.05 with the relaxation times $\tau_{\perp} = 2.9$, 5.6, and 10 ns, respectively. For the two longest polymers, a stretched exponential behavior was obtained.

In the following, the length of the attachment phase and how it scales with the chain length are more closely examined. For that reason, the subsequent labeling is made: $t_{\text{attach}}^{\text{start}}$ as the start and $t_{\text{attach}}^{\text{end}}$ as the end of the attachment region employing the time dependence of $\langle R_g^2(t)\rangle_{\perp}^{1/2}$ as shown in the inset of Figure 6 using a logarithmic time scale. Figure 6 displays $t_{\text{attach}}^{\text{start}}$ and $t_{\text{attach}}^{\text{end}}$ as a function of N in a double-logarithmic representation. If the time interval between these is identified as $\tau_{\text{attach}} = t_{\text{attach}}^{\text{end}} - t_{\text{attach}}^{\text{start}}$, it is evident that there is a $\tau_{\text{attach}} \sim N^{\beta}$ dependence with $\beta \approx 0.65$.

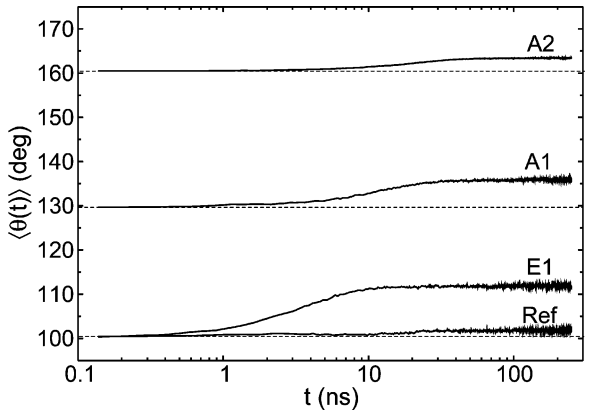

Figure 9. Average angle formed by three consecutive beads $\langle\theta(t)\rangle$ as a function of time t for the reference system (Ref), the semiflexible polymer (A1), the stiff polymer (A2), and the polymer with the stronger bead−surface attraction (E1) during adsorption.

Figure 5b shows that the spreading of the chain over the surface starts at a later time for longer polymers. As already alluded to, it is clear that the asymptotic limit of $\langle R_g^2(t)\rangle_{\parallel}^{1/2}$ is not reached for chains with $N \geq 40$. The start of the spreading of the chain on the surface $t_{\text{spread}}^{\text{start}}$ has been extracted from $\langle R_g^2(t)\rangle_{\parallel}^{1/2}$ in a way similar to the determination of $t_{\text{attach}}^{\text{start}}$. Figure 6 also displays $t_{\text{spread}}^{\text{start}}$ as a function of N. It can thus be concluded that for the shortest polymer ($N = 40$) the chain contraction perpendicular to the surface and the spreading on the surface start at the same time. However, as the polymer becomes longer, the onset of the spreading occurs after the perpendicular contraction has started.

Finally, Figure 5c shows that this increased time separation of the perpendicular contraction and the spreading on the surface led to a deeper minimum of the reduced chain size occurring at longer times as expressed by $\langle R_g^2(t)\rangle^{1/2}$. In absolute length scale, the increase of this depth at increasing N becomes even larger.

6.3. Variation of Chain Stiffness and Bead−Surface Potential. As well as the reference system (Ref), systems with a polymer having a larger persistence length (A1 and A2) and systems with an increased bead−surface attraction (E1) will be considered (see Table 2). Throughout, the polymer consists of $N = 40$ beads.

Figure 7 shows the center of mass during the adsorption process for the four different systems. First, it can be noticed that the initial location of the center of mass for the semiflexible (A1) and stiff (A2) chains is further away from the surface as compared to the reference system. This is a consequence of the preparation of the initial state for the BD simulations, as already discussed. The inset of Figure 7 shows that the initial diffusion rate of the polymer toward the surface is only weakly affected by its stiffness. Regarding the system with the stronger bead−surface attraction (E1), the initial diffusion toward the surface is the same as for the reference system but soon becomes faster, owing to the stronger bead−surface attraction. At equilibrium, the location of the center of mass varies among the systems. This is mainly a consequence of different extensions of the chain perpendicular to the surface.

The normalized rms radius of gyration and its two projections are shown in Figure 8. The general behavior at increasing chain stiffness and stronger bead−surface attraction is similar to that of the reference system but differs in several aspects.

An elongation of the chain perpendicular to the surface, as deduced from $\langle R_g^2(t)\rangle_{\perp}^{1/2}$, also appears for the semiflexible and stiff chains (Figure 8a). The stronger bead−surface attraction makes this effect more pronounced. At equilibrium, the per-

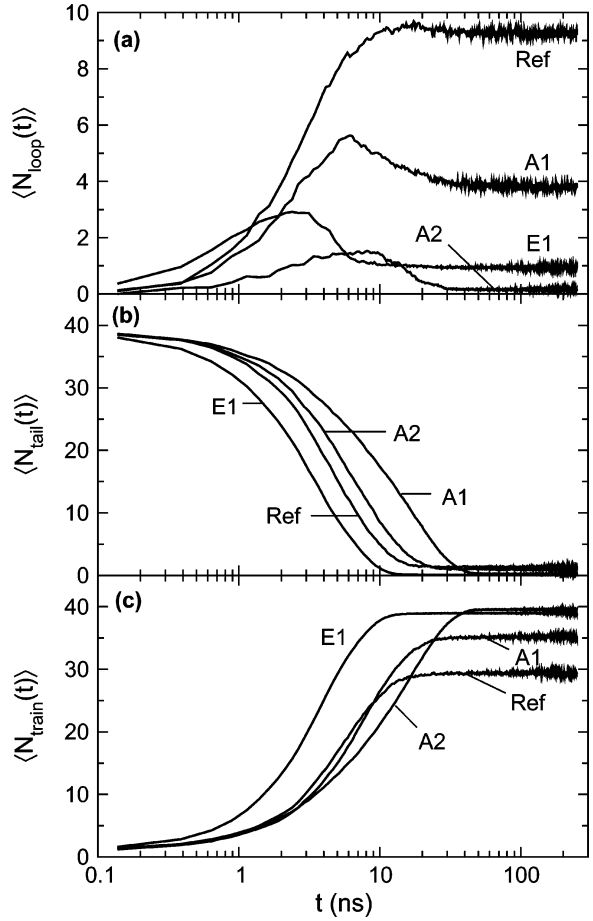

Figure 10. Average total number of beads in (a) loops, (b) tails, and (c) trains, $\langle N_\alpha(t)\rangle$, $\alpha = \{\text{loop, tail, train}\}$ as a function of time t for the reference system (Ref), the semiflexible polymer (A1), the stiff polymer (A2), and the polymer with the stronger bead−surface attraction (E1) during adsorption.

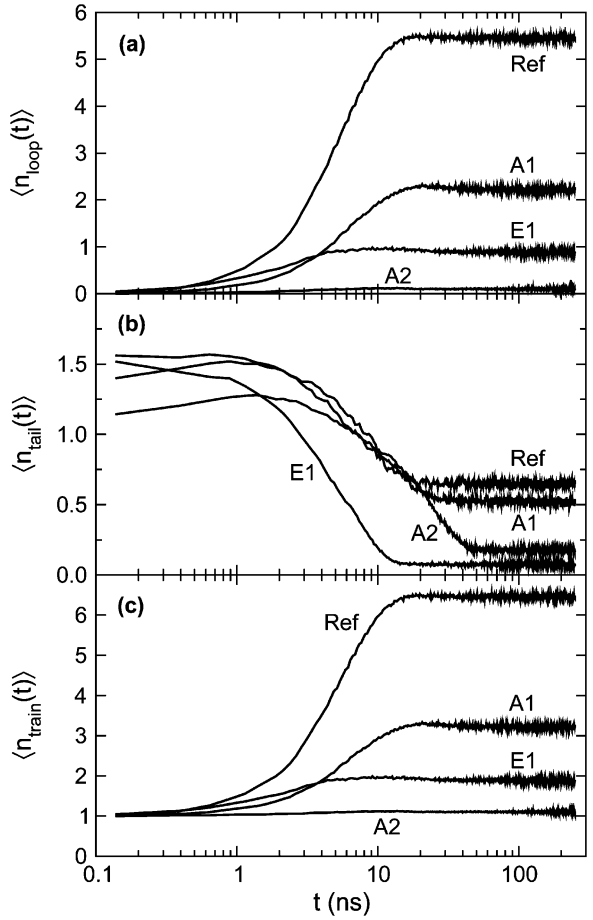

Figure 11. Average number of (a) loops, (b) tails, and (c) trains, $\langle n_\alpha(t)\rangle$, $\alpha = \{\text{loop, tail, train}\}$, as a function of time t for the reference system (Ref), the semiflexible polymer (A1), the stiff polymer (A2), and the polymer with the stronger bead−surface attraction (E1) during adsorption.

pendicular chain extension becomes smaller at increasing stiffness and increasing bead−surface attraction. In the former case, the increased chain rigidity suppresses the fluctuations of the chain conformations, and in the latter case the narrower bead−surface potential well has the same effect. This flattening of the chain causes the center of mass to be located closer to the surface. Previous MD simulations[10] and MC simulations[13] have also demonstrated flatter polymer configurations for more rigid chains in the vicinity of an attractive surface.

The dynamics of the spreading as described by $\langle R_g^2(t)\rangle_\parallel^{1/2}$ are given in Figure 8b. A similar analysis as previously made for the different chain lengths shows that the onset of the chain extension parallel to the surface for the semiflexible and stiff chains appears after the perpendicular contraction has started ($t_{\text{spread}}^{\text{start}} > t_{\text{attach}}^{\text{start}}$) as for the reference chain. However, and in particular for the stiffest chain, the mechanism is different; here, there is a preferential orientation of the stiff chain rather than an extension of a coil. For the system with the stronger bead−surface attraction, $t_{\text{spread}}^{\text{start}} = 3$ ns $< t_{\text{attach}}^{\text{start}} = 4$ ns. Hence, the spreading starts to appear before the chain contracts perpendicular to the surface. This suggests that the dynamics (stretching, attachment, and subsequent spreading) of this part of the chain become sufficiently fast such that a clearer distinction between the dynamics of this and remaining parts of the polymer occurs. Despite the earlier completion of the perpendicular contraction (smaller $t_{\text{attach}}^{\text{end}}$) and the earlier start of the spreading appearing for the stronger bead−surface attraction, the time for reaching equilibrium is similar to that for the reference system (Figure 8b). The more strongly adsorbed polymer is more restricted to a quasi-two-dimensional motion, thus requiring a longer time to structurally relax.[17,18] The slowing down of the spreading is anticipated to become more pronounced as the surface becomes rough. Thus, it can be concluded that the spreading depends not only on the vertical structure of the surface but also on the magnitude of the bead−surface interaction.

Similar to the reference system, $\langle R_g^2(t)\rangle^{1/2}$ values for the semiflexible and stiff chains also display a minimum due to the partial time displacement of the opposing behavior of $\langle R_g^2(t)\rangle_\perp^{1/2}$ and $\langle R_g^2(t)\rangle_\parallel^{1/2}$ (Figure 8c). However, the relatively early increase of $\langle R_g^2(t)\rangle_\parallel^{1/2}$ makes $\langle R_g^2(t)\rangle^{1/2}$ smoother for the E1 system.

Figure 9 displays the time dependence of the average angle formed by three consecutive bonds (bond angle) in the chain during the adsorption process. For the reference system, this angle remains essentially constant throughout the adsorption process. In contrast, the semiflexible (A1) and stiff (A2) chains as well as the system with the stronger bead−surface attraction (E1) all show an increased bond angle, occurring mainly in the attachment phase. The straightening of the bond angle is substantial for the semiflexible chain and smaller for the stiff one. The largest straightening appears for the E1 chain. Hence, the transition from a 3- to 2-dimensional coil with the concomitantly increasing excluded volume effects may significantly straighten the bond angle.

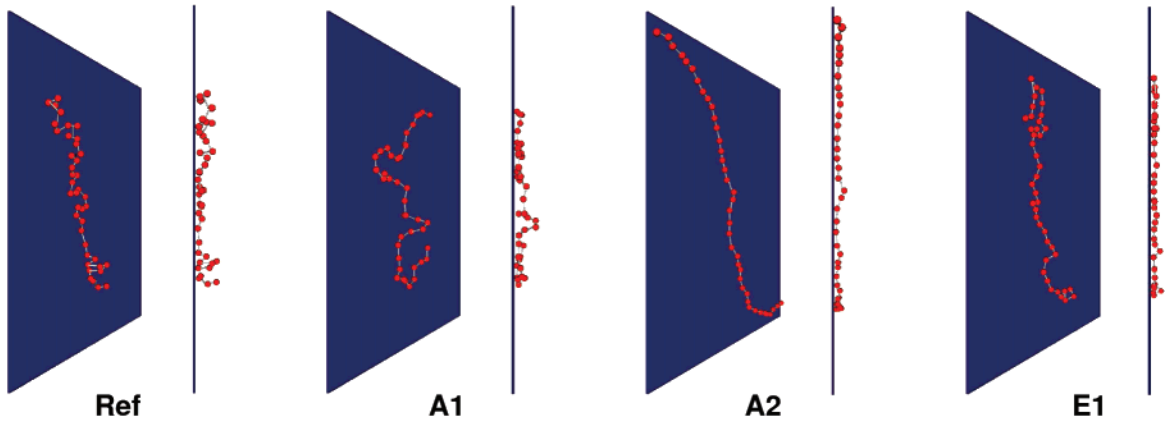

Figure 12. Snapshots of final adsorbed states from BD simulations visualized from front and side for the reference system (Ref), the semiflexible polymer (A1), the stiff polymer (A2), and the polymer with the stronger bead−surface attraction (E1).

The time evolution of the average number of beads residing in loops, tails, and trains is given in Figure 10, and Figure 11 displays the number of these subchains in adsorbed chains. As for the reference system, all changes in the loop, tail, and train characteristics are completed in the attachment phase. Furthermore, the data are consistent with a faster attachment process at the stronger bead−surface attraction.

In more detail, Figure 10a shows that the number of beads located in loops passes through a maximum during the adsorption process for all except the reference system. Moreover, Figure 11a reveals that the number of loops increases throughout the attachment phase. Hence, it can be concluded that the maximum in $\langle N_{loop}(t)\rangle$ arises from a reduction of the number of beads in a loop during the later part of the attachment phase. This is driven either by the chain stiffness (systems A1 and A2) or by the stronger bead−surface attraction (system E1). At equilibrium, the stiff chain essentially does not contain any loops, and the chain with the stronger bead−surface attraction contains only on the average one loop having one bead.

For all systems, the number of beads residing in tails is a decreasing function of time. At equilibrium, $\langle N_{tail}\rangle$ is two or below. The number of these short tails $\langle n_{tail}\rangle$ decreases with increasing chain stiffness and bead−surface attraction. In systems A2 and E1, the average number of tails is below 0.2.

Finally, the number of beads in trains increases continuously with time. Whereas the fraction $\langle N_{train}\rangle/N$ amounts to 0.75 for the reference system, it becomes ≈0.98 for systems A2 and E1. This increase in the number of beads in trains is accompanied by a decrease in the number of tails $\langle n_{tails}\rangle$. For the stiff chain, essentially only one train appears. The mechanism for formation of trains on the surface has earlier been reported by Ponomarev et al.[26] for polymers undergoing adsorption with high bead−surface attraction. The "zipping" of the chain onto the surface reported by Ponomarev seems to be a likely mechanism not only for the systems with a higher bead−surface attraction but also for the stiffer polymers as well. Snapshots of typical final adsorbed states of the Ref, A1, A2, and E1 systems are given in Figure 12. With the reference system as the point of departure, the different conformational characteristics of the stiffer chains and the chain with a higher bead−surface attraction are clearly distinguishable.

In summary, the bare chain persistence length and the strength of the bead−surface attraction have a decisive influence on the adsorption dynamics and the final structure of the adsorbed polymer. The semiflexible and stiff chains exhibit a flatter conformation as compared to the flexible chain. With a stronger bead−surface attraction, the attachment becomes faster, whereas the relaxation of the adsorbed chains becomes slower. An increased bead−surface attraction also leads to a flatter and more extended chain conformation of the adsorbed polymer.

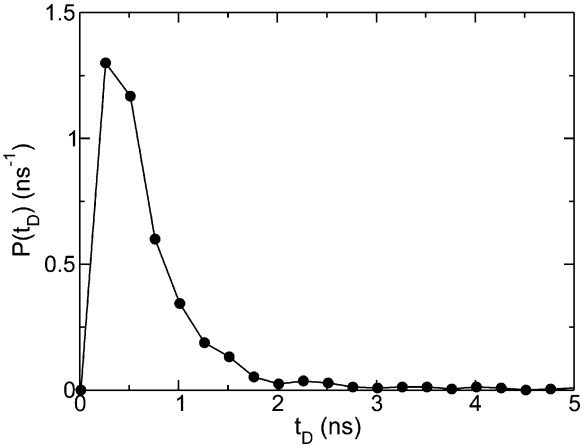

Figure 13. Normalized probability distribution $P(t_D)$ of detachment time t_D for an adsorbed polymer for the reference system.

7. Desorption

In the following section the desorption process occurring after the attractive bead−surface interaction is made repulsive for the reference system is examined. Since different bead−surface interactions are involved, the desorption process is not the reverse of the adsorption process. The desorption is driven by an increasing configurational chain entropy, whereas the adsorption gains enthalpy by having the polymer adsorbed to the surface. A potential way to experimentally realize a related desorption process would be to adsorb a long and weak polyion and thereafter change the solution pH using a flow cell.

Figure 13 shows the normalized probability $P(t_D)$ of the time t_D required for the chain to detach from the surface under the present conditions. This probability also displays a prominent peak followed by a tail. The integral of $P(t_D)$ shows that 85% of the chains have detached after 1.2 ns. Hence, the process involving a complete detachment is 1 order of magnitude faster than the attachment phase of the full adsorption process.

The time evolution of the center of mass and the extension of the chain during the desorption are given in Figure 14. In Figure 14a, $\langle \Delta z_{com}(t)\rangle^2 = \langle z_{com}(t) - z_{com}(0)\rangle^2$ is displayed. Two phases can be found: one initial, extending up to $t \approx 50$ ns, and thereafter a second one where $\langle \Delta z_{com}(t)\rangle^2$ increases linearly with t, consistent with a free diffusion. From the self-diffusion equation for a semiinfinite space, the propagator $P(z, t; z = 0,$

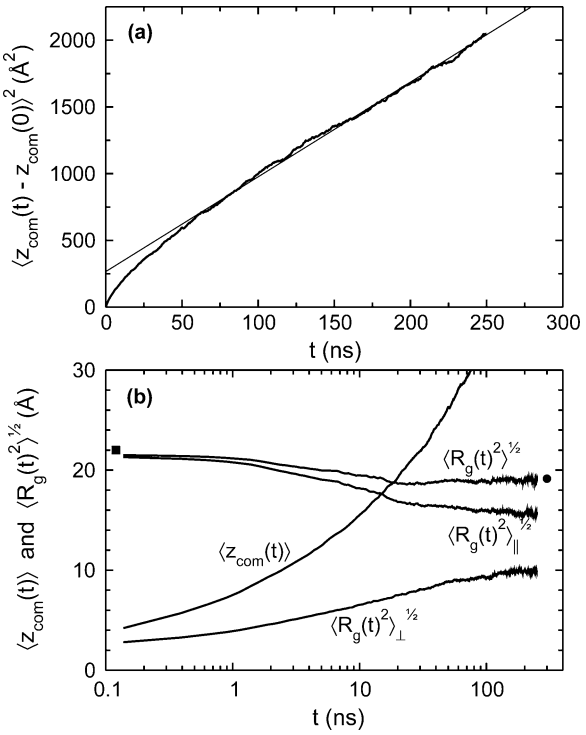

Figure 14. (a) Square mean displacement in the z-direction $\langle z_{com}(t) - z_{com}(0)\rangle^2$ and (b) center of mass $\langle z_{com}(t)\rangle$, rms radius of gyration $\langle R_g^2(t)\rangle^{1/2}$, and its two projections $\langle R_g^2(t)\rangle_\perp^{1/2}$ and $\langle R_g^2(t)\rangle_\|^{1/2}$ as a function of time t for the reference system during desorption. Rms radii of gyration for free polymer (circle) and adsorbed polymer (square) obtained from MC simulations are also shown.

$t = 0) = (1/\pi Dt)^{1/2} \exp(-z^2/4Dt)$, $z \geq 0$, is obtained, which gives $\langle z(t)\rangle^2 = 4Dt/\pi$. Equalizing the slope in Figure 14a with $4D/\pi$, we obtain the self-diffusion coefficient $D = 5.6$ Å^2/ns for the coil, which is twice as large as that obtained from the bulk simulations. At the end of the simulations $\langle z_{com}(t)\rangle = 47$ Å, well away from the surface.

Figure 14b shows that during the desorption process $\langle R_g^2(t)\rangle_\perp^{1/2}$ increases and $\langle R_g^2(t)\rangle_\|^{1/2}$ decreases during the same time frame with similar rates. This is in contrast to the adsorption process where changes in $\langle R_g^2(t)\rangle_\perp^{1/2}$ and $\langle R_g^2(t)\rangle_\|^{1/2}$ to a large degree occurred sequentially in time. However, equilibrium shape has not yet been attained after 250 ns, since neither $\langle R_g^2(t)\rangle_\|^{1/2}$ nor $\langle R_g^2(t)\rangle_\perp^{1/2}$ has completely leveled out. Moreover, their ratio is 1.6 at $t = 250$ ns as compared to $(2)^{1/2} \approx 1.4$ at equilibrium. Nevertheless, the overall extension of the coil as measured by $\langle R_g^2\rangle^{1/2}$ reaches its final value, as predicted from the MC simulations (solid square), already at $t \approx 20$ ns.

Figure 15 displays the time development of the loop, tail, and train characteristics during the desorption process. An initial comparison with Figure 4 shows that these changes are similar but appear obviously in a reversed order. The number of beads in trains $\langle N_{train}(t)\rangle$ and the number of trains $\langle n_{train}(t)\rangle$ decrease, whereas the number of beads in loops $\langle N_{loop}(t)\rangle$ and the length of loops $\langle L_{loop}(t)\rangle$ first increase, peak, and then decrease. Finally, the number of beads in tails $\langle N_{tail}(t)\rangle$ and the length of the tails $\langle L_{tail}(t)\rangle$ increase continuously until the polymer is desorbed.

In more detail, it can be observed that already at the shortest time displayed $\langle N_{loop}(t)\rangle$ has increased from 10 to 20 beads and that $\langle L_{loop}(t)\rangle$ peaks at 7. Hence, the loops are much more significant during the desorption than during the adsorption process. Furthermore, $\langle n_{loop}(t)\rangle$ is also initially increased before steadily decreasing and finally leveling off. This is understood as follows. Before the desorption starts, the chain is adsorbed

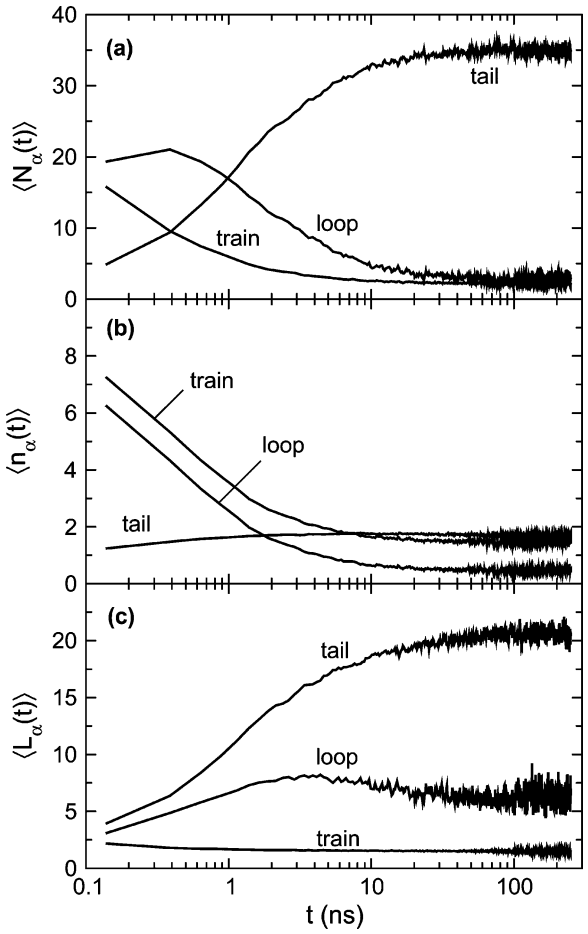

Figure 15. (a) Average total number of beads in loops, tails, and trains $\langle N_\alpha(t)\rangle$, (b) average number of loops, tails, and trains $\langle n_\alpha(t)\rangle$, and (c) average number of beads in a loop, tail, and train $\langle L_\alpha(t)\rangle$, $\alpha = \{$loop, tail, train$\}$ as a function of time t for the reference system during desorption.

in an extended state, where nearly all beads are in contact with the surface. As the attractive bead−surface interaction is switched off, all beads are affected simultaneously. Hence, loops start to be formed along the whole chain. Initially, the fraction of beads being in loops increases as beads are released from the surface. When the number of trains starts to decrease significantly, (i) loops are merged making the remaining loops longer and (ii) loops and tails are merged, making the number of beads residing in tails larger and those in loops smaller. On the contrary, during the adsorption, parts of the chain are rather sequentially brought into contact with the surface. The bead−surface attraction is comparably strong, leading to the formation of extended trains and short loops. Hence, the conformational changes during the adsorption and desorption are different.

8. Conclusions

Brownian dynamics simulations have been employed to investigate dynamical aspects of adsorption of uncharged polymers onto planar surfaces from solution. The polymers were released at a short separation from the surface, and their location and conformation were analyzed during the adsorption process. Monte Carlo Metropolis simulations were used to generate initial chain conformations and to establish equilibrium structures of the adsorbed state.

On the basis of the dynamics obtained from a reference system involving the adsorption of a flexible chain with 40 beads and an intermediate adsorption strength, the adsorption process can be divided into three phases:

(1) Distortion phase. In this phase, the polymer approaches the surface and becomes deformed by its interaction with the surface. The part of the coil nearest the surface becomes elongated perpendicular to the surface.

(2) Attachment phase. This phase starts with a physical contact between the polymer and the surface, which is followed by a relatively fast reduction in the extension perpendicular to the surface and a start of the spreading of the polymer on the surface. The radius of gyration displayed a nonmonotonous variation due to the initial polymer stretching and a partly time-separated variation in the perpendicular and parallel extension. Large changes in the loop, tail, and train characteristics appear and are completed in the attachment phase.

(3) Relaxation phase. During the last phase, the polymer continues to spread on the surface. This spreading constitutes the slowest process of establishing the adsorbed equilibrium structure.

The adsorption process for polymers up to $N = 640$ beads has been examined. Naturally, the dynamics become slower with longer polymers. The characteristic time of the attachment phase increased sublinearly in N, whereas the time to obtain complete structural relaxation displayed a much stronger N dependence. In fact, it was so slow that the full relaxation was not reached for $N \geq 80$. Hence, the time separation of the perpendicular and parallel extension increases with polymer length.

The characteristic features of the adsorption process of two less flexible chains remained essentially the same as those for the flexible one, although the relaxed adsorbed states displayed considerable structural differences. In particular, the loop, tails, and train characteristics showed a tighter bound polymer as the stiffness is increased.

With increasing bead−surface attraction, the length of the attachment phase was reduced, but the relaxation phase still remained long. As for the stiffer chains, the adsorbed state was characterized by a large number of beads being in trains and only a few in loops. The number of beads in tails remained low as in the reference system. This strong attachment makes the polymer 2-dimensional and contributes to the slowing down of the spreading dynamics.

Finally, the desorption of adsorbed chains after an instantaneous removal of the attractive component of the bead−surface attraction was also investigated. The rms radius of gyration and its two components displayed monotonous variations with time. The desorption is characterized by a simultaneous detachment along the whole chain, as opposed to the adsorption where sections of the chain were sequentially adsorbed.

Acknowledgment. The authors thank Dr. Peter Sellers for helpful discussions and linguistic insight and the Center for Scientific and Technical Computing at Lund University (LUNARC) for generous allocation of computational resources. This work was supported by grants from the Swedish Research Council (VR).

References and Notes

(1) Fleer, G. J.; Lyklema, J. In *Adsorption From Solution at the Solid/Liquid Interface*; Academic Press: New York, 1983.
(2) Evans, D. F.; Wennerström, H. *The Colloidal Domain: Where Physics, Chemistry, Biology and Technology Meet*, 2nd ed.; Wiley-VCH: New York, 1999.
(3) Fleer, G. J.; Cohen Stuart, M. A.; Scheutjens, J. H. M. H.; Cosgrove, T.; Vincent, B. *Polymers at Interfaces*; Chapman & Hall: London, 1993.
(4) Norde, W. *Colloids and Interfaces in Life Sciences*; Marcell Dekker: New York, 2003.
(5) Douglas, J. F.; Johnson, H. E.; Granick, S. *Science* **1993**, *262*, 2010.
(6) Hasegawa, R.; Doi, M. *Macromolecules* **1997**, *30*, 3086.
(7) Eisenriegler, E.; Kremer, K.; Binder, K. *J. Chem. Phys.* **1982**, *77*, 6296.
(8) Bishop, M.; Clarke, J. H. R. *J. Chem. Phys.* **1990**, *93* (2), 1455.
(9) Konstadinidis, K.; Prager, S.; Tirrell, M. *J. Chem. Phys.* **1992**, *97*, 7777.
(10) Kramarenko, E. Y.; Winkler, R. G.; Khalatur, P. G.; Khokhlov, A. R.; Reineker, P. *J. Chem. Phys.* **1996**, *104*, 4806.
(11) Sumithra, K.; Baumgaertner, A. *J. Chem. Phys.* **1999**, *110*, 2727.
(12) Striolo, A.; Prausnitz, J. M. *J. Chem. Phys.* **2001**, *114*, 8565.
(13) Sintes, T.; Sumithra, K.; Straube, E. *Macromolecules* **2001**, *34*, 1352.
(14) Sikorski, A. *Macromol. Theory Simul.* **2002**, *11*, 359.
(15) Bachmann, M.; Janke, W. *Phys. Rev. E* **2006**, *73*, 041802.
(16) Xia, T. K.; Landman, U. *Science* **1993**, *261*, 1310.
(17) Shaffer, J. S. *Macromolecules* **1994**, *27*, 2987.
(18) Lai, P. Y. *J. Chem. Phys.* **1995**, *103*, 5742.
(19) Wang, Y.; Rajagopalan, R.; Mattice, W. L. *Phys. Rev. Lett.* **1995**, *74*, 2503.
(20) Wang, Y.; Rajagopalan, R. *J. Chem. Phys.* **1996**, *105*, 696.
(21) Zajac, R.; Chakrabarti, A. *J. Chem. Phys.* **1996**, *104*, 2418.
(22) Milchev, A.; Binder, K. *Macromolecules* **1996**, *29*, 343.
(23) Pandey, R. B.; Milchev, A.; Binder, K. *Macromolecules* **1997**, *30*, 1194.
(24) Liu, H.; Chakrabarti, A. *Polymer* **1999**, *40*, 7285.
(25) Takeuchi, H. *Macromol. Theory Simul.* **1999**, *8*, 391.
(26) Ponomarev, A. L.; Sewell, T. D.; Durning, C. J. *Macromolecules* **2000**, *33*, 2662.
(27) Baschnagel, J.; Mayer, H.; Varnik, F.; Metzger, S.; Aichele, M.; Müller, M.; Binder, K. *Interface Sci.* **2003**, *11*, 159.
(28) Wolterink, J. K.; Barkema, G. T.; Cohen Stuart, M. A. *Macromolecules* **2005**, *38*, 2009.
(29) Gray, J. J. *Curr. Opin. Struct. Biol.* **2004**, *14*, 110.
(30) Cohen Stuart, M. A.; Hoogendam, C. W.; de Kaiser, A. *J. Phys.: Condens. Matter* **1997**, *9*, 7767.
(31) Ellis, M.; Kong, C. Y.; Muthukumar, M. *J. Chem. Phys.* **2000**, *112*, 8723.
(32) Dias, R. S.; Pais, A. A. C. C.; Linse, P.; Miguel, M. G.; Lindman, B. *J. Phys. Chem. B* **2005**, *109*, 11781.
(33) Kiriy, A.; Gorodyska, G.; Minko, S.; Tsitsilianis, C.; Jaeger, W.; Stamm, M. *J. Am. Chem. Soc.* **2003**, *125*, 11202.
(34) Ullner, M.; Jönsson, B.; Peterson, C.; Sommelius, O.; Söderberg, B. *J. Chem. Phys.* **1997**, *107*, 1279.
(35) Akinchina, A.; Linse, P. *Macromolecules* **2002**, *35*, 5183.
(36) Ermak, D. L.; McCammon, J. A. *J. Chem. Phys.* **1978**, *69*, 1352.
(37) Allen, M. P.; Tildesley, D. J. *Computer Simulations of Liquids*; Oxford University Press: Oxford, England, 1987.
(38) Linse, P. MOLSIM, Version 4.0, Lund University, Sweden, 2004.
(39) Le Guillou, J. C.; Zinn-Justin, J. *Phys. Rev. Lett.* **1977**, *39*, 95.

MA0702602